Oceanic response to changes in the WAIS and astronomical forcing during the MIS31 superinterglacial

Flavio Justino[1], Douglas Lindemann[1], Fred Kucharski[2], Aaron Wilson[3], David Bromwich[3], and Frode Stordal[4]

[1]Department of Agricultural Engineering, Universidade Federal de Vicosa, PH Rolfs, Vicosa, Brazil
[2]The Abdus Salam International Centre for Theoretical Physics, Trieste, Italy
[3]Polar Meteorology Group, Byrd Polar and Climate Research Center, The Ohio State University, Columbus, OH, USA
[4]University of Oslo,Department of Geosciences, Forskningsparken Gaustadalleen, Oslo, Norway

Correspondence to: Flavio Justino (fjustino@ufv.br)

Abstract. The Marine Isotope Stage 31 (MIS31, between 1085 ka and 1055 ka) was characterised by higher extra-tropical air temperatures and a substantial recession of polar glaciers compared to today. Paleoreconstructions and model simulations have increased the understanding of the MIS31 interval, but questions remain regarding the role of the Atlantic and Pacific Oceans in modifying the climate associated with the variations in Earth's orbital parameters. Multi-century coupled climate simulations, with the astronomical configuration of the MIS31 and modified West Antarctic Ice Sheet (WAIS) topography, show an increase in the thermohaline flux and northward oceanic heat transport (OHT) in the Pacific Ocean. These oceanic changes are driven by anomalous atmospheric circulation and increased surface salinity in concert with a stronger meridional overturning circulation (MOC). The intensified northward OHT is responsible for up to 85% of the global OHT anomalies and contributes to the overall reduction in sea-ice in the Northern Hemisphere (NH) due to Earth's astronomical configuration. The relative contributions of the Atlantic Ocean to global OHT and MOC anomalies are minor compared to that of the Pacific. However, sea-ice changes are remarkable, highlighted by decreased (increased) cover in Ross (Weddell) Sea but widespread reductions of sea-ice across the NH.

1 Introduction

Recent paleoreconstructions and climate modeling experiments have attempted to disentangle the influence of dominant forcing on past climates from, orbital configurations (Yin, 2013; Erb et al., 2015) to the El Niño-Southern Oscillation (ENSO) and ice sheet variability (Russon et al., 2011; DeConto et al., 2012). However, other issues like the air-sea coupling and its impact on atmospheric and oceanic variability (Knutti et al., 2004; Bush and Philander, 1998) require additional scrutiny. This two-way interaction implies that the atmosphere affects the sea-surface conditions by modifying oceanic heat fluxes which in turn feed back into the lower tropospheric atmospheric flow (Timmermann et al., 1998).

The global climate response to these processes is governed by complex interactions occurring not only at the air-sea interface but also in sub-surface oceanic layers where a substantial amount of heat is stored (Ganachaud and Wunsch, 2003; Meehl et al., 2011; Yin and Berger, 2012). Therefore, fully coupled models are essential to reproduce the large-scale climatic features

of these glacial/interglacial regimes (Otto-Bliesner et al., 2003; Erb et al., 2015). This is especially true when evaluating the climate response to potential changes in the meridional overturning circulation (MOC) and the oceanic heat transport (OHT) (Shin et al., 2003). Increased OHT from the Pacific into the Arctic associated with changes in Antarctic ice volume has been argued to affect the Beringian climate during interglacial epochs (Coletti et al., 2015) as well as maintain warm high-latitude oceanic surface temperatures in many intervals throughout the geologic past (Comeau et al., 2016).

Others have taken advantage of simplified climate models using an atmospheric general circulation model (GCM) coupled to slab mixed-layer ocean model (e.g., Coletti et al., 2015; Roychowdhury and DeConto, 2016; Lunt et al., 2017). Though valid, this modeling approach reduces ocean-atmosphere feedbacks that are crucial for the reorganization of atmospheric flow on long timescales. It has been emphasized by coupled modeling studies that oceanic dynamical changes related to orbital fluctuations are the primary forcing in determining large-scale atmospheric flow patterns (Erb et al., 2015; Tomas et al., 2016). Because oceanic dynamical changes during interglacial intervals are important for determining the large-scale atmospheric circulation and temperature distribution (Coletti et al., 2015), answers to these issues are pursued here by employing the International Centre for Theoretical Physics - Coupled Global Climate Model (ICTP-CGCM) (Kucharski et al., 2015).

An interesting test case to explore these climate feedbacks is the Marine Isotope Stage 31 interval (MIS31) which occurred at $\sim$ 1080 ka BP (Lisiecki and Raymo, 2005). This epoch has been characterized by warmer global air temperatures and substantial melting of polar glaciers compared to today (Melles et al., 2012; Wet et al., 2016). However, paleoreconstructions and modeling results disagree with respect to the North Hemisphere (NH) warming during the MIS31, suggesting the need for a better understanding of this interglacial and other warmer climates as discussed by Melles et al. (2012) and Coletti et al. (2015). .

Analyses have focused on the climate response to individual drivers of the interglacial climates (Knorr and Lohmann, 2014; Yin and Berger, 2012; Pollard and DeConto, 2009; Villa et al., 2008). Among other effects, insolation has been shown to play the dominant role in defining high-northern latitude temperature and sea ice (Yin and Berger, 2012). The longitude of the perihelion (precession) is also found to lead changes in the equatorial Pacific seasonal cycle (Erb et al., 2015). Meanwhile, past fluctuations in atmospheric CO2 concentration have been claimed to induce long-term surface and deep-water temperature trends (Knorr and Lohmann, 2014). Accordingly, this study aims to disentangle the individual contributions of the West Antarctic Ice Sheet (WAIS) and the astronomical configuration during the MIS31 interglacial climate by applying a coupled climate model. Mechanisms related to the combined effects of these forcing on MIS31 climate are explored, including the inter-hemispheric coupling, the potential role of OHT, and wind-driven and thermohaline changes in oceanic circulation.

2 Coupled model and experimental design

The coupled climate model utilized is the ICTP-CGCM, consisting of the atmospheric global climate model "SPEEDY" version 41 (Kucharski et al., 2006) coupled to the Nucleus for European Modelling of the Ocean (NEMO) model (Madec, 2008) with the OASIS3 coupler (Valcke, 2013). The atmospheric component runs at T30 horizontal resolution and there are eight levels in

the vertical. The model includes physically-based parameterizations of large-scale condensation, shallow and deep convection, shortwave and longwave radiation, surface fluxes of momentum, heat and moisture, and vertical diffusion.

NEMO is a primitive equation z-level ocean model based on the hydrostatic and Boussinesq approximations. This version applies a horizontal resolution of 2° and a tropical refinement to 0.5°. The ocean component has 31 vertical levels with layer thicknesses ranging from 10 m at the surface to 500 m at the ocean bottom (16 levels in the upper 200 m). Additional details of the ICTP-CGCM are described by Justino et al. (2015) and Kucharski et al. (2015).

The ICTP-CGCM control simulation (CTR) is run under present day orbital forcing for over 2000 years since proper evaluations of long-term ocean-atmosphere processes require statistical equilibrium representation of the climate state, particularly for paleoclimatic features in a coupled atmosphere-ocean model (Peltier and Solheim, 2004). The CO_2 concentration in our CTR climate is 325 ppm as it characterizes anthropogenic emission of CO_2 by the year 1950 but does not include the accelerated increase that occurred by the end of the 20th century.

2.1 Model performance of the CTR climate

To evaluate the reliability of the ICTP-CGCM to represent the present day climate (control run), Fig. 1 shows Sea Suface Temperature (SST) differences between the CTR run and the NOAA Optimum Interpolation (OI) SST V2 (NOAA-OI-SST-V2) (Reynolds et al., 2002) and sea-ice area based on the Hadley Centre Sea Ice and SST data set (HadISST) (Rayner et al., 2003). The control run has been simulated for 1000 years and CTR climatology is based on the last 100 years. The modeled evaporation minus precipitation (E - P) flux is compared to the Interim Reanalysis from the European Centre for Medium-Range Weather Forecasts (ECMWF) ERA-Interim (ERAI) (Dee et al., 2011). (Kucharski et al., 2015) have provided detailed analyses of the present day climate simulated by the ICTP-CGCM.

Figure 1a shows annual SSTs in the ICTP-CGCM are colder than NOAA-OI-SST-V2 and are related to differences in the lower tropospheric flow. In fact, the zonal wind over the NH storm track region in ICTP-CGCM as well as over the Southern Hemisphere (SH) polar jet are weaker than in ERAI up to $\pm$ 4m/s. In the NH during the summer season, this is associated with reduced temperature advection from Asia and North America onto the North Atlantic and Pacific leading to lower ICTP-CGCM SSTs. However, it should be stressed that overall SST differences are in the range of $\pm$ 2°C.

Analysis of E - P flux demonstrates that our coupled model reproduce the main characteristics of the ERAI E - P flux (Fig. 1b), but the zonal averages reveal that the ICTP-CGCM is wetter than the ERAI in the equatorial belt and SH mid-latitudes (not shown). However, differences are less than 1 mm day^{-1}. This implies that the E - P flux associated with the Intertropical Convergence Zone (ITCZ) needs improvements in order to better reproduce equatorial climate dynamics including decreased precipitation in the Pacific Warm Pool and over the southern part of the South Atlantic. Nevertheless, this is a recurrent feature in other CGCMs (Jia-Jin, 2007)

Comparison of the ICTP-CGCM sea-ice area with estimates from the Hadley Centre counterpart shows that the ICTP-CGCM does a reasonable job in both hemispheres for December-January-February (DJF) and June-July-August (JJA) (Table 1). Sea-ice area is computed as the total area covered by ice, which corresponds to sum of the area of each cell multiplied by the fractional concentration for that cell. Insofar as annual mean conditions are concerned (Fig. 1c and 1d), limitations are

evident as ICTP-CGCM is dominated by higher sea-ice concentration than demonstrated by the Hadley Center across most of the NH, in particularly in the Russian Arctic (Fig. 1c). In the SH, our model shows lower concentration of ice in the Atlantic polar region but higher concentration in the sea-ice edge in extra-tropical latitudes around 60°S and near the Ross Sea (Fig. 1d). The ICTP-CGCM exhibits higher amplitude in the seasonal cycle of sea-ice thickness in the Weddell Sea compared to HadISST, with thinner sea-ice in summer (not shown).

Several investigations have demonstrated that extra-tropical SST and sea ice are currently among the largest limitations in Earth climate modeling. Based on the Coordinated Ocean-ice Reference Experiments (CORE) model inter-comparison, Griffies et al. (2009) found that models generally have large biases in all fields such as SST, sea surface salinity (SSS), sea ice, and zonal velocity in the equatorial Pacific subsurface. Though models show a substantial spread in skill depicting the Atlantic Meridional Overturning Circulation (AMOC), Kiel-ORCA performs very well. The ICTP-CGCM, which is a coupled ocean-atmosphere model, applies the same Kiel-ORCA ocean component, and the ICTP-CGCM biases are in the lower range compared to other CORE models.

The importance of the air-sea coupling at the atmosphere-ocean interface has long been recognized, and the impacts on the Ekman layer must be accounted for in models. CGCMs driven by a low resolution oceanic component are very limited in their ability to reproduce the wind-driven upwelling, and therefore are warmer than models of higher resolution. More importantly, low resolution atmosphere-ocean models struggle to reproduce the OHT. Thus, these models simulate weaker AMOC, allowing a larger storage of heat in the SH due to the NH heat piracy assumption (Broecker, 1998).

3 Design of the sensitive experiments

To evaluate the impacts on climate due to changes in the WAIS topography and the astronomical forcing during the MIS31 interglacial, three additional sensitivity experiments have been conducted. Analyses have been carried out for the last 100 years of these 1000 year-long simulations. The astronomical forcing is assumed to represent 1072 ka based on the warmest summer month in the Lake El'gygytgyn reconstruction (Coletti et al., 2015; Melles et al., 2012) (Table 1 supp. material):

1. TOPO - applies the MIS31 WAIS topography as proposed by previous studies (Pollard and DeConto, 2009; Justino et al., 2015);
2. AST - conducted with astronomical configuration characteristic of the 1072 ka (Berger, 1978; Coletti et al., 2015);
3. MIS31 - the combined effect of the forcing described in TOPO and AST.

In all sensitivity experiments the CO2 concentration is set to 325 ppm. For the MIS31 interval this is reasonable based on boron isotopes in planktonic foraminifera shells (Honisch et al., 2009). The CO2 concentration during the MIS31 could have varied between 300 and 350 ppm due to propagated error of the individual pH, SST, salinity, and alkalinity in the reconstructions. This variation in the amount of atmospheric CO2 may lead to an overestimation in the NH warming as simulated in our study. Changes in CO2 by about +50 ppm may be associated with +0.3 K change in globally averaged surface temperature, but

this change in temperature is within the uncertainty of the climate sensitivity (Bindoff et al., 2013). The concentration of CH4 (N2O) is 800 (288) ppb (Schilt et al., 2010; Loulergue et al., 2008), values similar to those proposed by Coletti et al. (2015).

Since the Greenland Ice Sheet (GIS) was only slightly smaller during MIS5e than current conditions (Dahl-Jensen et al., 2013) and Coletti et al. (2015) showed that MIS5e and MIS31 differed by only 0.6°C, the GIS in our MIS31 simulations reflects present day conditions. However, our simulation does not include changes in oceanic gateways, because there is no conclusive global land-sea mask reconstruction for the MIS31 interval. The WAIS topography has been modified, but no changes in sea level have been applied in our modeling experiment. The modified WAIS does reflect sea water albedo in the sensitivity runs. Changes in the initial salinity field in response to the WAIS collapse have not been included either. Aiken (2008) demonstrated limited response of the climate system to the freshening implied by Antarctic sea-ice melt, even in the presence of adding a much larger freshwater forcing of approximately 0.4 Sv. Moreover, Vaughan and Arthern (2007) argued that an outflow rate associated with WAIS melting is not realistically attainable, making it difficult to implement in a freshwater forcing experiment. Insofar as the WAIS collapse is concerned, this study focuses on analyzing the climate response to mechanical changes in orography. Our simulation does not include changes in oceanic gateways, because there is no conclusive global land-sea mask reconstruction for the MIS31 interval. The WAIS topography has been modified, but no changes in sea level have been applied in our modeling experiment. However, the modified WAIS reflects sea water albedo in the sensitivity runs. Changes in the initial salinity field in response to the WAIS collapse have not been included. Aiken (2008) demonstrated limited response of the climate system to the freshening implied by Antarctic sea-ice melt, even in the presence of adding much larger freshwater forcing of approximately 0.4 Sv. Moreover, Vaughan and Arthern (2007) argued that an outflow rate associated with WAIS melting is not realistically attainable, making it difficult to implement in a rose experiment. Insofar as the WAIS collapse is concerned this study focuses on analysing the climate response to mechanical changes in orography.

4 Climate response to MIS31 forcing

4.1 The WAIS collapse

Previous work by Justino et al. (2015) using a simplified low resolution ocean model (3° × 3°) has demonstrated that the incorporation of a modified WAIS topography, characteristic of the MIS31 interval, results in generally warmer global surface temperatures as compared to current climate with enhanced positive anomalies between 50-70°S.

Under present-day conditions, katabatic winds flowing offshore from the continent over the Weddell Sea contribute to the maintainance cold air over the sea-ice edge (Mathiot et al., 2010). Modeled Weddell Sea warming in the TOPO simulation is related to weaker katabatic winds and reduced continental cold air advection due to a collapsed WAIS (Justino et al., 2015). During periods of reduced sea-ice thickness, there is an increase in the heat flux from the ocean to the atmosphere. This increases the convective mixing and warms the overlying atmosphere. Higher surface temperatures in the Ross Sea in TOPO than seen in the CTR simulation are supported by the Ocean Drilling Program (ODP) site 1165 and by the marine glacial record of the AND-1B sediment core in the Ross Ice Shelf (Naish et al., 2009).

The WAIS collapse also leads to cooling in the North Atlantic. Temperature anomalies of opposite sign between the North and South Atlantic have been a recurrent feature in the Earth's climate. This dipole is related to the North Atlantic freshening (Knutti et al., 2004) and associated with the modification of the SH wind patterns and subsequently wind-driven circulation (Speich et al., 2007). In both situations, changes involve anomalous patterns of OHT. Seasonal sea-ice changes (DJF and JJA) between TOPO and CTR show areal increases in both hemispheres with larger changes in the NH (Table 1). Annually–averaged sea-ice changes due to the WAIS collapse are noted in the Labrador and Nordic Seas that are statistically significant at 95

It should be noted that the warming indicated by the current ICTP-CGCM TOPO simulation (Fig. 2a) is substantially smaller than the results presented by Justino et al. (2015). There are several factors related to these differences. Justino et al. (2015) show much weaker SH westerly flow that leads to warmer SSTs across the high latitudes of the SH compared to the present study (not shown). The previous study also reflects weaker teleconnections between the tropical and extra-tropical regions related to the ENSO (Severijns and Hazeleger, 2010). NEMO (present model) and CLIO (previous model) are characterized by drastically modified ENSO related-tropical variability in terms of variance and magnitude (Severijns and Hazeleger, 2010; Park et al., 2009). The NEMO ocean model used in the present study properly simulates the global oceanic features as it resolves convective and mesoscale processes in the mixed layer and thermohaline related to the ENSO.

4.2 The Astronomical forcing

Turning to the impact of astronomical changes on global surface temperatures (AST minus CTR), warming is evident in the northeastern Pacific and Atlantic Oceans (Fig. 2b). The orbital forcing during the MIS31 reflects high obliquity and eccentricity, enhancing boreal summer insolation. Downward solar radiation differences at the top of the atmosphere between AST and CTR reach values of up to 50 W m^2 at 60°N (not shown). In fact, increased heat in the oceanic surface layer during the summer months hinders the winter cooling and hampers sea-ice cover over extra-tropical latitudes (Yin and Berger, 2012; Alexander et al., 1999). Thus, vigorous oceanic heat exchange in AST leads to higher near-surface air temperatures compared to the CTR run. Seasonal changes project onto annual conditions due to the remnant insolation effect that is stronger during the NH summertime (Yin and Berger, 2012).

Indeed, the NH (SH) warming (cooling) is primarily associated with intensified (weakened) summer insolation that is dominant in the polar and subtropical regions. In addition to reduced insolation in the SH, stronger atmospheric circulation (southeast trade winds and westerlies) lead to lower surface temperatures due to stronger equatorial upwelling and modified Ekman dynamics (McCreary and Lu, 1994). The wind-evaporation-SST feedback also plays a role due to modification in the latent heat through evaporation (Wang et al., 1999).

Elsewhere, the atmospheric circulation and the heat exchanges associated with air-sea interactions determine annual mean conditions. The incorporation of the astronomical forcing also exhibits anomalous SSTs in such a way that the Atlantic Ocean anomalies resemble present-day conditions under the positive phase of the Atlantic Multidecadal Oscillation (AMO) (Delworth and Mann, 2000). SST anomalies in the North Pacific on the other hand, depict the warm phase of the Pacific Decadal Oscillation (PDO) (Zhang et al., 1997). Therefore, these climate modes of variability (AMO and PDO) may be characteristic of a global climate governed by an excess of heat in the NH as occurred in the MIS31 interval. The 20th century climate,

which experienced larger changes in NH temperatures compared to the SH (Kang et al., 2015), also resulted from the influence of the AMO and PDO on temperature anomalies. In today's climate, the NH warming arises in part because of northward cross-equatorial OHT (Kang et al., 2015); however, the heat transport must be intensified under external forcing characteristic of interglacial climates.

Table 1 and Fig. 2e demonstrate that the inclusion of orbital forcing leads to decreased (increased) sea-ice area in the NH (SH) with statistically significant changes in the NH. The SH experiences a greater change during JJA. However, Fig. 2e shows that when annual average is assessed, most changes in the SH are significant and that the AST anomalous sea-ice pattern opposes the TOPO response in the Weddell and Bellingshausen Seas.

4.3 The MIS31 climate

The global climate response due to the combined effect of changing WAIS topography and astronomical forcing (MIS31 simulation) is primarily a result of changes in the latter forcing, as Fig. 2c shows a similar SST anomaly pattern as Fig. 2b. Nevertheless, the combined forcing appears not to be linear in the vicinity of Antarctica (Supplementary Fig. 2). Linearity is noted, however, by intensified warming in the Ross Sea as a result of warmer SSTs in TOPO and AST compared to the CTR climate. Non-linearity is shown through reduced cooling in the Weddell Sea in the MIS31 simulation compared to the AST simulation (Supplementary Fig. 2). This is related to the absence of the WAIS topography that reduces the strong cooling associated with changes in the astronomical forcing. Comparison between the MIS31 and the AST runs can be indirectly used to further identify the effect of the WAIS topography in the SH sea-ice changes (Figs. 2e and 2f). The anomalous SST patterns in the NH are also associated with modified air-sea coupling, in particular reduced Ekman drift and reduced evaporative cooling in concert with the MIS31 orbital forcing. Indeed, stronger mid-latitude and polar westerlies over the Kuroshio/Oyashio region and weaker northeast trade winds over the central-eastern Pacific (not shown) result in higher SSTs and sea-ice anomalies in the respective regions (Table 1, Fig. 2).

Modification of the WAIS topography is associated with changes in sea-ice area, particularly in the Atlantic Ocean. Changes in the astronomical forcing on the other hand are more responsible for climate anomalies on a global perspective. *Differences between MIS31 and AST usefully demonstrate that the substantial reduction of sea-ice cover in the Ross Sea and in some extent changes in Weddell Sea are substantially affected by the WAIS collapse (Supplementary Fig. 1c). Specifically, the MIS31 simulation is warmer in the Weddell and Ross Seas by up to 1.5°C with respect to AST, which is accompanied by an approximately 10% reduction in sea-ice cover. In fact, the individual influence of the collapse of WAIS in MIS31 is more evident in the Bellingshausen Sea (Figs. 2e and 2f). In the NH, the removal of WAIS and orbital forcing act in opposite directions for sea-ice changes.*

The sensitivity experiments demonstrate that compared to CTR, warmer SSTs and reduced sea-ice are only simulated in the Ross Sea region. This is in agreement with the Cape Roberts Project-1 results and data from the Antarctic Geological Drilling project (ANDRILL) (Naish et al., 2009) (Fig. 2). In fact, outside of the Ross Sea, Antarctic sea-ice during the MIS31 interval

may have been more abundant compared to current conditions. In the NH, sea-ice cover is substantially reduced by up to 15% in DJF and by up to 50% in the AST and MIS31 runs in JJA (Table 1).

In order to provide a quantitative comparison between global temperature reconstructions and our modeling results, multiple proxies are used (Wet et al., 2016). Table 2 shows 15 sites distributed throughout both hemispheres (Supplementary Fig. 3). Reconstructed temperature values in Table 2 have been extracted by drawing an orthogonal line to the time series with an intersection at approximately 1070 Ka of Fig. 5 by Wet et al. (2016)). In the NH, the model is colder than reconstructed temperatures (2-3°C) in extra-tropical latitudes, namely at the Lake E and ODP 982 sites (Table 2; (Melles et al., 2012; Lawrence et al., 2009)).

These locations are dominated by extreme seasonality that may not be fully captured in the ICTP-CGCM. Over extra-tropical regions, heat advection embedded in storms has been pointed to as an important contributor for defining temperature and weather patterns over those regions (Lehmann and Coumou, 2015; Jost et al., 2005; Kageyama and Valdes, 2000). Storm tracks are tightly connected to the meridional thermal gradient, and over the continent, more frequent cold spells in winter are related to decreased storm track activity (Lehmann and Coumou, 2015). Lower resolution models such as the atmospheric component in the ICTP-CGCM may limit the ability to represent both the structure and intensity of the storms passing over East Asia and the North Atlantic. Subsequently, weaker storms may induce colder temperatures at the Lake E and ODP 982 sites. Elsewhere in the NH, differences are less than 1°C (Raymo et al., 1996; Li et al., 2011; Herbert et al., 2010a; Naafs et al., 2013).

In the equatorial regions, the model performs well compared to reconstructed temperatures with departures up to $\pm$ 1°C (McClymont and Rosell-Melé, 2005; Medina-Elizalde et al., 2008; Herbert et al., 2010b, 2010c; Li et al., 2011; Russon et al., 2011; Dyez and Ravelo, 2014). Comparing ODP sites 849, 847, 846 and 871 in the equatorial Pacific (Table 2), the east-west SST gradient may be identified as supported by changes in the zonal circulation. Indeed, the MIS31 climate experiences weaker trade winds, consistent with Martínez-Garcia et al. (2010). The ODP sites in the SH also corroborate with previous results showing small differences between model and reconstructions (Table 2; Scherer et al., 2008; Voelker et al., 2015; Naish et al., 2009; Russon et al., 2011; McClymont et al., 2005; Crundwell et al., 2008; Martínez-Garcia et al., 2010).

4.4 Changes in MOC and OHT

There is particular interest in evaluating changes to the MOC associated with warming and/or freshening of the NH high-latitude surface waters due to natural variability, and/or including anthropogenic induced-global warming (Rahmstorf et al., 2015). The AMOC is a key element of the climate system, because it carries a substantial amount of heat poleward, and on long timescales, AMOC plays an important role in coupling the SH and NH (Broecker, 1998).

The ICTP-CGCM AMOC exhibits values that closely match observations (Kanzow et al., 2010; Ferrari and Ferreira, 2011; Talley et al., 2003) as well as higher resolution models (Stepanov and Haines, 2014). Consequently, a fair representation of the AMOC should lead to proper OHT estimates under present day conditions, because the majority of the OHT is driven by the AMOC. Moreover, the resolution of ICTP-CGCM across the tropics is sufficient enough to capture the majority of the OHT for the globe.

The Antarctic bottom-water (AABW) is closely related to sea-ice processes that involve brine release due to sea-ice formation and winds (Stössel et al., 1998). Despite limitations in reproducing the sea-ice seasonal features in the ICTP-CGCM, simulated deep water formation in the SH occurs in both the Atlantic and Pacific Oceans (Figs. 3-4).

The AABW represented by our CTR run in the Atlantic attains values of about 5 Sv ($10^6 m^3 s^{-1}$), which is comparable to 8 Sv based on absolute geostrophic velocity from hydrographic data (Talley et al., 2003) and from climatological Ekman transports. At 25°S, the ICTP-CGCM delivers AABW in the Pacific Ocean up to 10 Sv also in line with Talley et al. (2003), and 6-8 Sv at 10°N matched values found by Wijffels et al. (1996).

Figures 3a and 3d show that compared to data-based estimates (Ganachaud and Wunsch, 2000), the ICTP-CGCM properly reproduces the magnitude of the North Atlantic Deep Water (NADW, 15 ± 2 Sv) at 2°N. The main sites of the NADW formation, namely Greenland-Iceland, Norwegian (GIN) and Labrador Seas (Wood et al., 1999) are also properly located as shown by analyses of the density contribution (Fig. 3a). Thermal changes dominate the NADW formation in comparison to the haline contribution. Indeed, a much colder extra-tropical atmosphere over the warmer ocean increases the vertical air-sea temperature contrast and consequently the ocean-atmosphere heat exchange (Schmitt et al., 1989; Speer and Tziperman, 1992). This leads to stronger convective mixing (Fig. 3a).

The modification of the WAIS results in a slightly reduced (but statistically significant) rate of formation of the NADW compared to the CTR (Fig. 3e). The weakening of the NADW in the TOPO simulation is associated with a reduction in the Labrador Sea surface salinity. Moreover, reduced heat exchange between the ocean and the atmosphere in the GIN Seas due to an increase in sea-ice plays a role (Table 1; Fig. 2d), thereby reducing convective mixing (Fig. 3b).

Changes in topography of the WAIS (Figs. 2 and 3) are stronger in the SH extra-tropics, and therefore, AST and MIS31 elsewhere show similar anomalous pattern in respect to the CTR simulation. Thus, we choose to show only results for MIS31. Figure 3c shows that despite reduced sea-ice compared to CTR, there is thermally-increased surface water density at the main sites of deep water formation in the MIS31 simulation, particularly in the Labrador and GIN seas (show as positive labels in Figs. 3c and 3f). Thus, the NADW in this experiment is deeper and more intense compared to CTR.

As shown by the thermal contribution, the acceleration of the MOC during the MIS31 simulation compared to the CTR simulation (Fig. 3f) is also a response to intensified westerly atmospheric flow across the northern North Atlantic (not shown). This leads to strong convective mixing. It can also be argued that less intrusion of the Antarctic water in the North Atlantic above 4000 m contributes to increased vertical instability favoring oceanic convection (Haupt and Seidov, 2012). This is opposite to findings concerning the Last Glacial Maximum (McManus et al., 2004; Peltier and Solheim, 2004), which assumes that a large intrusion of Antarctic water into the North Atlantic restricts most of the NADW into a shallower part of the ocean (Ballarotta et al., 2014).

The inclusion of MIS31 boundary conditions further affects the position of the main sites of deep water formation. Figure 3c shows that the convection sites in MIS31 have been shifted poleward compared to CTR. Labrador and GIN Seas concentrate a large amount of deep water formation. This occurs as a result of intensified surface wind field near 60°N (not shown), and subsequently leads to a strengthening of the subtropical gyre northward of its position in the CTR run. The North Atlantic also experiences increased salinity in the MIS31simulation compared to CTR, which is advected into the Labrador and GIN

Seas (Fig. 4d). An intensified MOC during the MIS31 and associated OHT have also been suggested by paleoreconstructions (Scherer et al., 2008) and have been claimed to prevent NH cooling during the MIS11 interval (Dickson et al., 2009). Figure 4a shows that our modeled OHT is in the range of global observations based on Ganachaud and Wunsch (2000, 2003). It should be noted as well that these observations exhibit large uncertainties in magnitude especially across the SH tropical region. These errors can be as large as 0.55 PW (petawatt) at 4.5°S and 0.6 PW at 1°S the Atlantic, which represent in some cases more than 60% of the total estimated OHT.

Insofar as the ICTP-CGCM is concerned (Fig. 4a), it underestimates the OHT in the NH due to its limitations in the Atlantic Ocean while the OHT in the Pacific is in the range/interval of values proposed by Ganachaud and Wunsch (2000, 2003). Between 20 and 30°N, where observations exhibit smaller errors, the model slightly overestimates the OHT in the Indian-Pacific region and underestimates in the Atlantic Ocean. These differences may be responsible for cooler modeled SSTs over the extra-tropical region of the North Atlantic compared to the ODP site 982. The OHT in the TOPO changes slightly compared to the CTR. However, in the AST and MIS31 simulations, a clear pattern of increased astronomically-driven northward OHT is present (Fig. 4a). In the mid-latitudes, an intensified atmospheric westerly flow in the vicinity of the American continent is simulated in the AST and MIS31 experiments. This contributes to an enhanced OHT via the transport of warmer subtropical water to mid-latitudes (Fig. 4a). As previously mentioned, southward transport between 0 and 1000 m in the NH mid-latitudes is reduced (Fig. 3f).

Interestingly, Fig. 4a also shows an essential contribution to global OHT anomalies from the Indian-Pacific since little difference in OHT is found across the Atlantic in the MIS31 simulation compared to CTR. This finding is in line with previous results demonstrating that increased OHT into the Arctic Ocean results in better correspondence between modeling results and the Lake E reconstruction (Coletti et al., 2015). Enhanced OHT during the MIS31 is also supported by the ODP site 846 (Herbert et al., 2010c) and 849 (McClymont and Rosell-Melé, 2005).

In order to investigate potential causes for the increased OHT in the MIS31 climate, Fig. 4 shows the sea surface salinity (SSS) and the vertical oceanic circulation pattern in the Pacific Ocean. Under CTR conditions, little North Pacific deep water forms (Fig. 4b). However, changes in the astronomical forcing induce modifications in the surface water density.

The density contribution (Fig. 3c) shows that the incorporation of the astronomical forcing leads to an increase in water density in the North Pacific and a simultaneous increased in SSS (see Fig. 4c). Moreover, the initial acceleration of the sub-tropical gyre associated with modified mid-latitude westerlies and the associated heat loss from the ocean to the atmosphere northward of 40°N also contribute to an increase in the surface density (Fig. 3c). Subsequently, this leads to the formation of the southward branch of the Pacific Meridional Overturning Circulation (PMOC; Fig. 4d).

Reduction in sea-ice cover reduces the density changes in the sea-ice/water interface, but this contribution to the PMOC weakening is marginal and confined to the Arctic region. Additional contribution to the PMOC is provided by increased E-P flux in AST and MIS31 runs compared to the CTR, which further increase the SSS in the North Pacific (Fig. 4b). Supplementary Fig. 5 summarizes the air-sea mechanisms which are involved in the PMOC formation rate. Evaluating the individual contributions of the wind-driven and thermohaline circulation to North Pacific OHT across 26°N shows that under CTR conditions from the surface to 300 m depth, the wind-driven component contributes up to 58% (0.55 PW) of the total OHT (not shown). These

values are similar to previous estimates based on observations (Talley, 2003). This demonstrates that in subtropics and mid-latitudes, most of the OHT is the result of the North Pacific gyre. An additional 42% (0.40 PW) of OHT occurs in the 300-1200 m layer.

For the MIS31 climate, the OHT associated with the wind-driven circulation (0-300 m) at 26°N is less than that of the CTR simulation and represents 44% of the total (55% in the CTR). This indicates that at this latitude, an important contribution to OHT is related to the thermohaline circulation below the Ekman layer. Compared to the CTR simulation, this represents an increase of 16%, from 40% in the CTR to 56% in the MIS31. It should to be mentioned however, that separating the thermohaline and wind-driven contributions should be interpreted carefully, as the wind-driven density transport partly drives the thermohaline circulation (Talley, 2003).

As shown by vertically integrating the zonal and meridional OHT at the basin scale, the contribution of the gyre circulation is dominant in particular between 30-45°N (Supplementary Figs. 2a and 2c). Under MIS31 conditions, zonally induced OHT is even stronger (Supplementary Fig. 2b), but northward of 45°N the role of the meridional contribution should be taken into account (Supplementary Fig. 2d). Hence, the evaluation of the OHT in a single longitudinal belt does not fully describe the OHT picture insofar as the characteristics of large scale domains are needed.

5 Summary and Concluding Remarks

Based on coupled climate simulations performed under present day and boundary conditions representative of the Marine Isotope Stage 31 (MIS31), our analyses provide evidence that under MIS31 climate conditions there was a remarkable reduction in sea-ice distribution across the NH due to the astronomical configuration of that epoch. This contrasts with increases in sea-ice area across the SH. The climate response to collapsing the WAIS is prominent in the vicinity of the Antarctic continent, whereas the effect of modification in the Earth orbital configuration extends worldwide.

It has furthermore been demonstrated that the MIS31 interglacial experienced significant changes in the Meridional Overturning Circulation (MOC). In the Atlantic, increases in the MOC are related to an intensified westerly atmospheric flow in the northern North Atlantic leading to strong convective mixing. The main convection sites in MIS31 have also been shifted poleward compared to the control simulation (CTR) in concert with changes in the position of the meridional thermal gradient.

Increased water density due to surface salinity changes and the acceleration of the subtropical gyre associated with modified mid-latitude westerlies in the MIS31 climate are responsible for modifying the convection in the North Pacific, resulting in the existence of a southward meridional thermohaline flow (PMOC). We suggest that this feature and associated OHT (Fig. 4a) play key roles in the NH warming during the MIS31 interval, as suggested by paleoreconstructions.

These modeling results have enormous implications for paleoreconstructions of the MIS31 climate that mostly assume overall ice free conditions in the vicinity of the Antarctic continent. Since these reconstructions may depict dominant signals in a particular time interval and locale, they cannot be assumed to geographically represent large-scale domains. Therefore, their ability to reproduce long-term environmental conditions should be considered with care. Finally, it is important to emphasize that understanding past interglacial intervals that are characterized by a depleted WAIS can shed light on the potential effects of

increasing atmospheric CO2, as the stability of the WAIS will be a key climate factor in decades to come (DeConto and Pollard, 2016; Nicolas et al., 2017).

Author contributions. F. Justino designed the study, wrote large portions of the manuscript and performed, data processing and plotting. D. Lindemann and F. Kucharski performed all model simulations. All authors substantially contributed to interpretation of the results.

Competing interests. The authors declare that they have no competing financial interests.

Acknowledgements. This work was supported by the the Brazilian National Research Council projects 232718/2014-8 and 407681/2013-2. The first author also thank the Byrd Polar and Climate Research Center for providing the necessary infrastructure.

. NOAA-OI-surface temperature-V2 and ICOADS data are provided by the NOAA/OAR/ESRL PSD, Boulder, Colorado, USA, from their Web site at http://www.esrl.noaa.gov/psd/. ERAI E - P flux was provided by the National Center for Atmospheric Research Staff (Eds),"The Climate Data Guide: ERA-Interim: derived components.", retrieved from https://climatedataguide.ucar.edu/climate-data/era-interim-derived-components, last modified 02 Jan 2014.

References

Aiken, C. M. M. H. E.: Sensitivity of the present-day climate to freshwater forcing associated with Antarctic sea ice loss, Journal of Climate, 21, 3936–3946, doi:10.1175/2007JCLI1901.1, 2008.

Berger, A.: Long-term variations of daily insolation and Quaternary climatic changes, Journal of the Atmospheric Sciences, 35, 2362–2367, doi:http://dx.doi.org/10.1175/1520-0469(1978)035<2362:LTVODI>2.0.CO;2, 1978.

Broecker, W.: Paleocean circulation during the last deglaciation. A bipolar seesaw?, Paleoceanography, 13, 119–121, 1998.

Coletti, A. J., DeConto, R. M., Brigham-Grette, J., and Melles, M.: A GCM comparison of Plio-Pleistocene interglacial-glacial periods in relation to Lake El'gygytgyn, NE Arctic Russia, Climate of the Past, 11, doi:10.5194/cpd-11-979-2015, 2015.

Crundwell, M., Scott, G., Naish, T., and Carter, L.: Glacial–interglacial ocean climate variability from planktonic foraminifera during the Mid-Pleistocene transition in the temperate Southwest Pacific, ODP Site 1123, Palaeogeography, Palaeoclimatology, Palaeoecology, 260, 202–229, 2008.

DeConto, R. M. and Pollard, D.: Contribution of Antarctica to past and future sea-level rise, Nature, 531, 591–597, 2016.

Dee, D. P., Uppala, S. M., Simmons, A. J., Berrisford, P., Poli, P., Kobayashi, S., Andrae, U., Balmaseda, M. A., Balsamo, G., Bauer, P., Bechtold, P., Beljaars, A. C. M., van de Berg, L., Bidlot, J., Bormann, N., Delsol, C., Dragani, R., Fuentes, M., Geer, A. J., Haimberger, L., Healy, S. B., Hersbach, H., Hólm, E. V., Isaksen, L., Kallberg, P., Ki ohler, M., Matricardi, M., McNally, A. P., Monge-Sanz, B. M., Morcrette, J.-J., Park, B.-K., Peubey, C., de Rosnay, P., Tavolato, C., Thépaut, J.-N., and Vitart, F.: The ERA-Interim reanalysis: configuration and performance of the data assimilation system, Quarterly Journal of the Royal Meteorological Society, 137, 553–597, doi:10.1002/qj.828, http://dx.doi.org/10.1002/qj.828, 2011.

Dyez, K. A. and Ravelo, A. C.: Dynamical changes in the tropical Pacific warm pool and zonal SST gradient during the Pleistocene, Geophysical Research Letters, 41, 7626–7633, doi:10.1002/2014GL061639, http://dx.doi.org/10.1002/2014GL061639, 2014GL061639, 2014.

Ganachaud, A. and Wunsch, C.: Large-scale ocean heat and freshwater transports during the World Ocean Circulation Experiment, Journal of Climate, 16, 696–705, 2003.

Herbert, T. D., Peterson, L. C., Lawrence, K. T., and Liu, Z.: Tropical ocean temperatures over the past 3.5 million years, Science, 328, 1530–1534, 2010a.

Herbert, T. D., Peterson, L. C., Lawrence, K. T., and Liu, Z.: Tropical ocean temperatures over the past 3.5 million years, Science, 328, 1530–1534, 2010b.

Herbert, T. D., Peterson, L. C., Lawrence, K. T., and Liu, Z.: Tropical ocean temperatures over the past 3.5 million years, Science, 328, 1530–1534, 2010c.

Jia-Jin, L.: The double-itcz problem in ipcc ar4 coupled gcms: ocean-atmosphere feedback analysis, Journal of Climate, 20, 4497–4525, doi:http://dx.doi.org/10.1175/JCLI4272.1, 2007.

Justino, F., Silva, A. S., Pereira, M. P., Stordal, F., Lindemann, D., and Kucharski, F.: The Large-Scale Climate in Response to the Retreat of the West Antarctic Ice Sheet, J. Climate, doi: http://dx.doi.org/10.1175/JCLI-D-14-00284.1, 2015.

Kucharski, F., Molteni, F., and Bracco, A.: Decadal interactions between the western tropical Pacific and the North Atlantic Oscillation, Clim. Dyn., 26, 79–91, 2006.

Kucharski, F., Ikram, F., Molteni, F., Farneti, R., Kang, I., No, H., King, M., Giuliani, G., and Mogensen, K.: Atlantic forcing of Pacific decadal variability, Climate Dynamics, 7, 1169–1188, doi:inpress, http://www.clim-past.net/7/1169/2011/, 2015.

Lawrence, K. T., Herbert, T. D., Brown, C. M., Raymo, M. E., and Haywood, A. M.: High-amplitude variations in North Atlantic sea surface temperature during the early Pliocene warm period, Paleoceanography, 24, n/a–n/a, doi:10.1029/2008PA001669, http://dx.doi.org/10.1029/2008PA001669, pA2218, 2009.

Li, L., Li, Q., Tian, J., Wang, P., Wang, H., and Liu, Z.: A 4-Ma record of thermal evolution in the tropical western Pacific and its implications on climate change, Earth and Planetary Science Letters, 309, 10–20, doi:10.1016/j.epsl.2011.04.016, 2011.

Madec, G.: NEMO: the OPA ocean engine, Note du Pole de Modelisation, pp. 1–110, Note du Pôle de modélisation de l'Institut Pierre-Simon Laplace No 27, http://dx.doi.org/10.1029/137GM07, 2008.

Martínez-Garcia, A., Rosell-Melé, A., McClymont, E. L., Gersonde, R., and Haug, G. H.: Subpolar link to the emergence of the modern equatorial Pacific cold tongue, Science, 328, 1550–1553, doi:10.1126/science.1184480, 2010.

Mathiot, P., Barnier, B., Gallée, H., nes, J. M. M., Sommer, J. L., Juza, M., and Penduff, T.: Introducing katabatic winds in global {ERA40} fields to simulate their impacts on the Southern Ocean and sea-ice, Ocean Modelling, 35, 146 – 160, doi:http://dx.doi.org/10.1016/j.ocemod.2010.07.001, http://www.sciencedirect.com/science/article/pii/S1463500310001022, 2010.

McClymont, E. L. and Rosell-Melé, A.: Links between the onset of modern Walker circulation and the mid-Pleistocene climate transition, Geology, 33, 389–392, 2005.

McClymont, E. L., Rosell-Melé, A., Giraudeau, J., Pierre, C., and Lloyd, J. M.: Alkenone and coccolith records of the mid-Pleistocene in the south-east Atlantic: implications for the index and South African climate, Quaternary Science Reviews, 24, 1559–1572, doi:10.1016/j.quascirev.2004.06.024, 2005.

McCreary, J. and Lu, P.: Interaction between the subtropical and the equatorial ocean circulations: The subtropical cell., J. Phys. Oceanogr., 24, 466–497, 1994.

Medina-Elizalde, M., Lea, D. W., and Fantle, M. S.: Implications of seawater Mg/Ca variability for Plio-Pleistocene tropical climate reconstruction, Earth and Planetary Science Letters, 269, 585–595, doi:10.1016/j.epsl.2008.03.014, 2008.

Melles, M., Brigham-Grette, J., Minyuk, P. S., Nowaczyk, N. R., Wennrich, V., DeConto, R. M., Anderson, P. M., Andreev, A. A., Coletti, A., Cook, T. L., Haltia-Hovi, E., Kukkonen, M., Lozhkin, A. V., Rosen, P., Tarasov, P., Vogel, H., and Wagner, B.: 2.8 Million Years of Arctic Climate Change from Lake El-gygytgyn, NE Russia, Science, 337, 315–320, doi:10.1126/science.1222135, http://www.sciencemag.org/content/337/6092/315.abstract, 2012.

Naafs, B. D. A., Hefter, J., Grützner, J., and Stein, R.: Warming of surface waters in the mid-latitude North Atlantic during Heinrich events, Paleoceanography, 28, 153–163, doi:10.1029/2012PA002354, http://dx.doi.org/10.1029/2012PA002354, 2013.

Nicolas, J. P., Vogelmann, A. M., Scott, R. C., Wilson, A. B., Cadeddu, M. P., Bromwich, D. H., Verlinde, J., Lubin, D., Russell, L. M., Jenkinson, C., et al.: January 2016 extensive summer melt in West Antarctica favoured by strong El Niño., Nature communications, 8, 15 799, 2017.

Peltier, W. and Solheim, L.: The climate of the Earth at Last Glacial Maximum: statistical equilibrium state and a mode of internal variability, Quaternary Science Reviews, pp. 335–357, 2004.

Pollard, D. and DeConto, R.: Modelling West Antarctic ice sheet growth and collapse through the past five million years, Nature, http://dx.doi.org/10.1038/nature07809, 2009.

Rahmstorf, S., Feulner, G., Mann, M. E., Robinson, A., Rutherford, S., and Schaffernicht, E. J.: Exceptional twentieth-century slowdown in Atlantic Ocean overturning circulation, Nature Climate Change, 5, 475–480, 2015.

Raymo, M., Grant, B., Horowitz, M., and Rau, G.: Mid-Pliocene warmth: stronger greenhouse and stronger conveyor, Marine Micropaleontology, 27, 313–326, 1996.

Rayner, N. A., Parker, D. E., Horton, E. B., Folland, C. K., Alexander, L. V., Rowell, D. P., Kent, E. C., and Kaplan, A.: Global analyses of sea surface temperature, sea ice, and night marine air temperature since the late nineteenth century, Journal of Geophysical Research: Atmospheres, 108, n/a–n/a, doi:10.1029/2002JD002670, http://dx.doi.org/10.1029/2002JD002670, 4407, 2003.

Reynolds, R. W., Rayner, N. A., Smith, T. M., Stokes, D. C., and Wang, W.: An improved in situ and satellite SST analysis for climate, Journal of climate, 15, 1609–1625, 2002.

Russon, T., Elliot, M., Sadekov, A., Cabioch, G., Corrège, T., and De Deckker, P.: The mid-Pleistocene transition in the subtropical southwest Pacific, Paleoceanography, 26, n/a–n/a, doi:10.1029/2010PA002019, http://dx.doi.org/10.1029/2010PA002019, pA1211, 2011.

Stössel, A., Kim, S.-J., and Drijfhout, S. S.: The impact of Southern Ocean sea ice in a global ocean model, Journal of physical oceanography, 28, 1999–2018, 1998.

Talley, D.: Shallow, intermediate, and deep overturning components of the global heat budget, J. Phys. Oceanogr., 35, 530–560, 2003.

Valcke, S.: The OASIS3 coupler: a European climate modelling community software, Geoscientific Model Development, 6, 373–388, doi:10.5194/gmd-6-373-2013, http://www.geosci-model-dev.net/6/373/2013/, 2013.

Vaughan, D. G. and Arthern, R.: Why Is It Hard to Predict the Future of Ice Sheets?, Science, 315, 1503–1504, doi:10.1126/science.1141111, http://www.sciencemag.org/content/315/5818/1503.short, 2007.

Wang, C., Weisberg, R. H., and Yang, H.: Effects of the wind speed-evaporation-SST feedback on the El Niño-Southern Oscillation, Journal of the atmospheric sciences, 56, 1391–1403, 1999.

Wet, G., Castañeda, I. S., DeConto, R. M., and Brigham-Grette, J.: A high-resolution mid-Pleistocene temperature record from Arctic Lake El'gygytgyn: a 50 kyr super interglacial from MIS 33 to MIS 31, Earth and Planetary Science Letters, 436, 56–63, 2016.

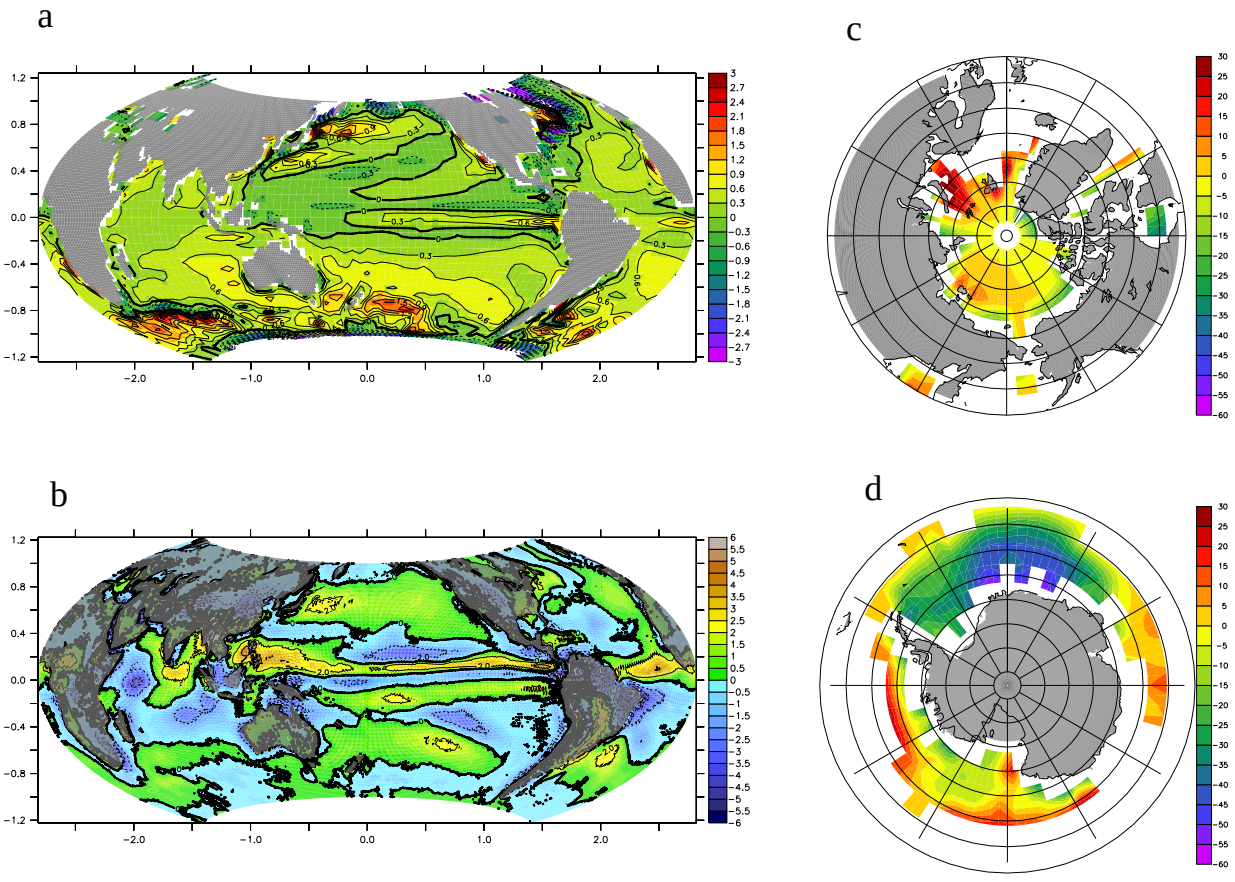

Figure 1. (a) Sea surface temperature differences (°C) between the CTR and the NOAA-OI-surface temperature-V2 . (b) E - P flux differences (mm day^{-1}) between the control simulation and the ERAI. Sea-ice area differences (%) between the CTR and the HadISST estimates, (c) Northern Hemisphere (d) Southern Hemisphere.

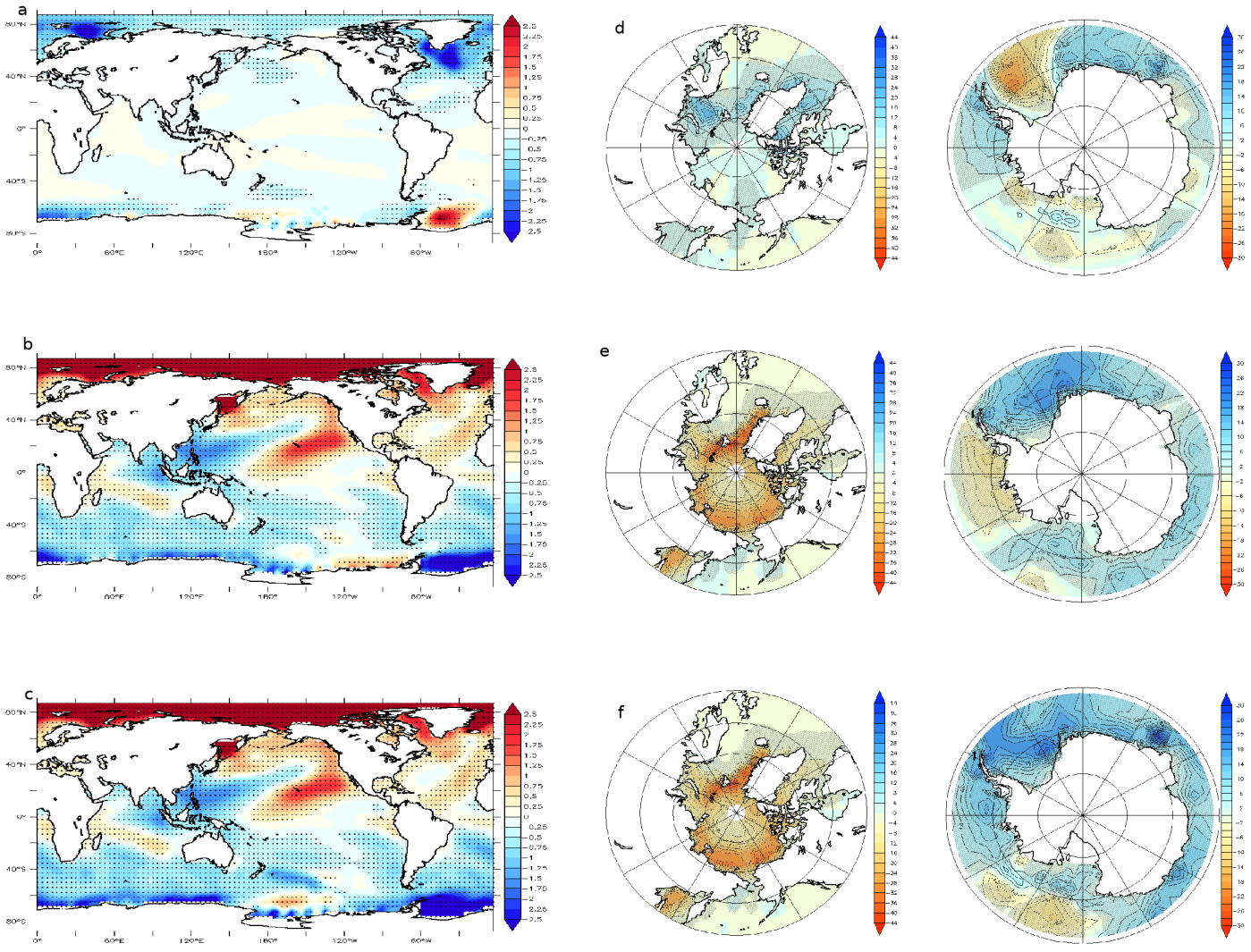

Figure 2. Surface temperature differences (°C) between (a) TOPO, (b) AST, and (c) MIS31 compared to the CTR. d), e) and f) are the same as a,b,c but for sea-ice differences (%). Dotted areas in a), b), and c) and hatched in d), e) and f) are significant at 95% based on t-test statistics.

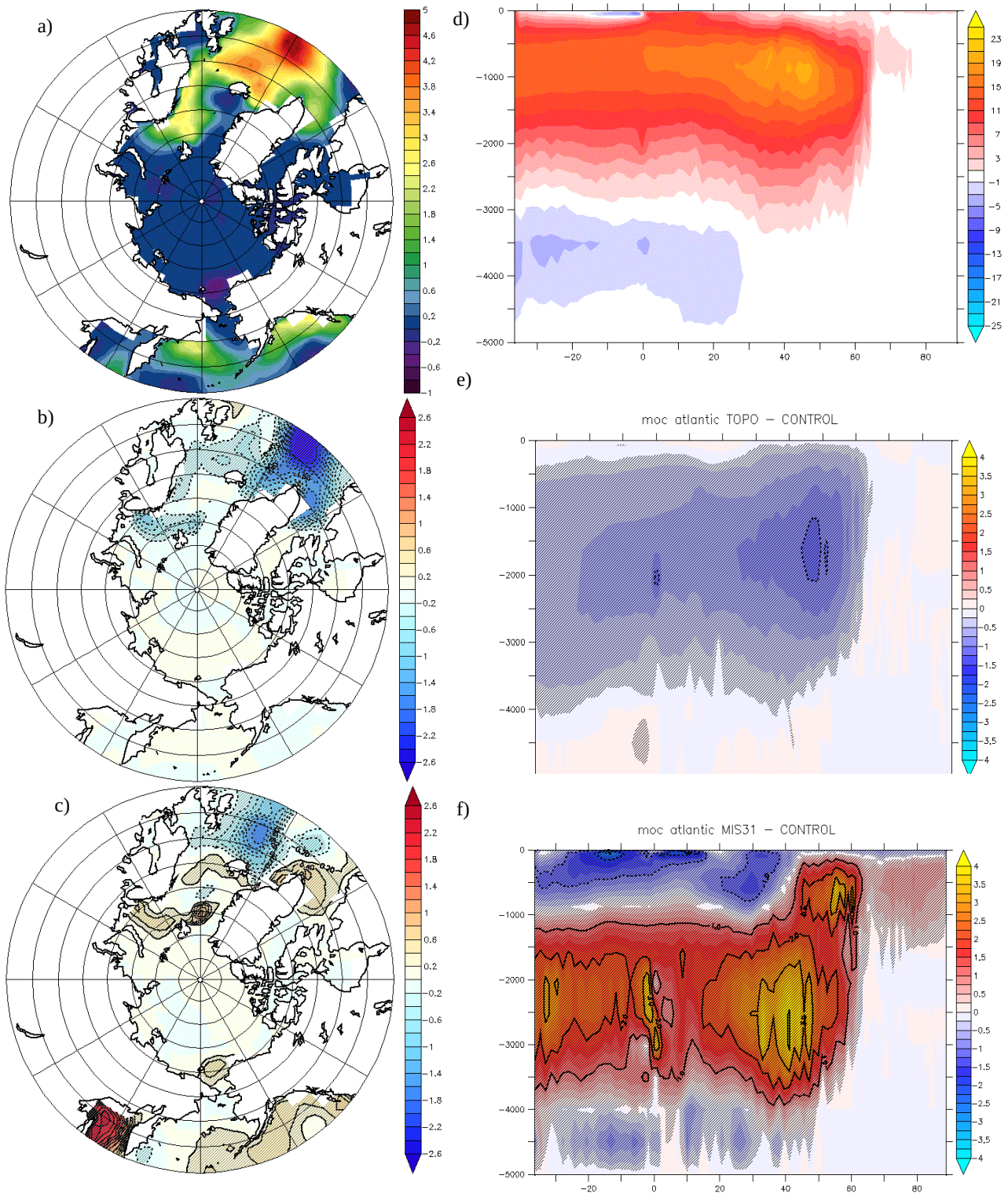

Figure 3. Density flux for CTR (a, $10^6 \mathrm{kgm}^{-2}\mathrm{s}^{-1}$) and differences between TOPO - CTR (b) and (c) MIS31 - CTR. (d) MOC (Sv) in the CTR and differences between the (e) TOPO - CTR and (f) MIS31 - CTR. Hatched areas are significant at 95% based on t-test statistics.

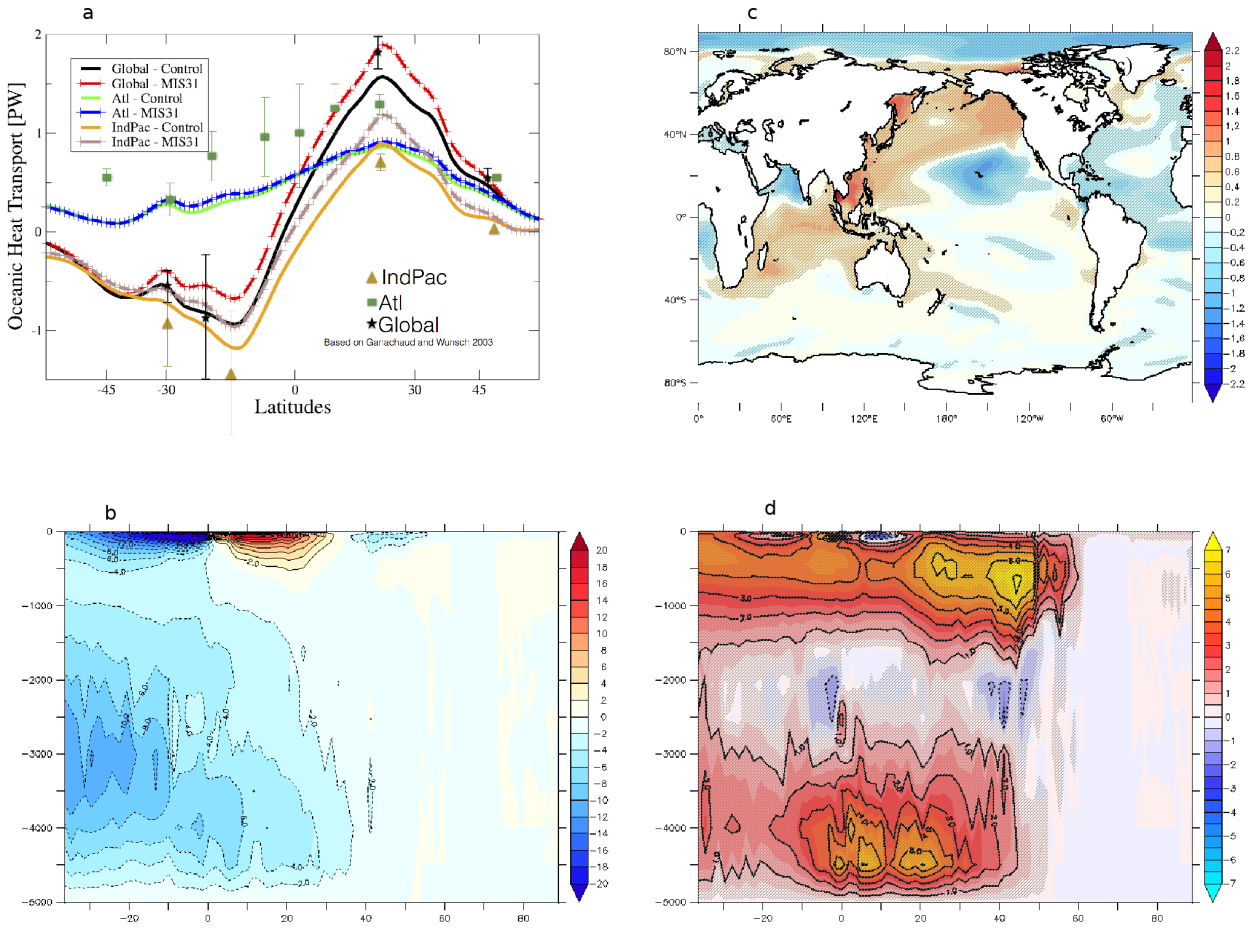

Figure 4. (a) Time-averaged OHT (PW) for CTR (solid line) and MIS31 (dashed-crossed line). Stars, squares and triagles show estimates based on Ganachaud and Wunsch (2003). (b) Pacific meridional stream-function (PMOC) in the CTR. (c) Sea surface salinity differences between MIS31 and CTR. (d) Differences between the MIS31 and CTR PMOC. Hatched regions in b) and dotted in c) are significant at 95% based on t-test statistics.

Table 1. Sea-ice area (10^9 m^2) in the NH and SH for Hadley Centre Sea Ice (in brackets), CTR and differences between the sensitivity experiments and CTR. Values with star are statistically significant at 95% based on t-test statistics.

	NH		SH	
	DJF	JJA	DJF	JJA
CTR (Hadley)	13.09 (13.36)	8.23 (8.68)	4.90 (5.10)	13.93 (13.08)
TOPO-CTR	0.8	0.5	0.03	0.4
AST-CTR	-1.3*	-4.0*	0.9	1.6
MIS31-CTR	-1.4*	-4.2*	1.3	2.3

Table 2. SST paleorecontruction and modeling inter-comparison. Values in Table 2 have been extracted by drawing orthogonal line to the timeseries with intersection at approximately the 1070 Ka, between the dashed lines of Figure 5 in Wet et al. (2016).

Site (coordinates)	Surf.Temp. (^{o}C) Reconstruction	Surf. Temp. (^{o}C) Speedy-NEMO	Differences between Speedy-NEMO and Reconstructions (^{o}C)	Reference
Lake E (67N 172E)	14.3	12.5	-2.2	(Melles et al., 2012)
ODP 982 (57N 15W)	13.8	10.8	-3.0	(Lawrence et al., 2009)
DSDP607 (41N 33W)	17.5	16.9	0.6	(Raymo et al., 1996)
306-U1313 (41N 32W)	18.0	16.9	-1.1	(Naafs et al., 2013)
1146 (19N 116E)	26.0	25.0	-1.0	(Herbert et al., 2010a)
722 (16N 59W)	27.0	28.0	1.0	(Herbert et al., 2010b)
1143 (9N 113E)	28.3	27.5	-0.8	(Li et al., 2011)
871 (5N 172E)	29.3	28.9	-0.4	(Dyez and Ravelo, 2014)
847 (0 95W)	25.6	25.0	-0.6	(Medina-Elizalde et al., 2008)
849 (0 110W)	25.8	25.0	-0.8	(McClymont and Rosell-Melé, 2005)
846 (3S 90W)	24.3	24.8	0.5	(Herbert et al., 2010c)
MD-06-301 (23S 166E)	25.0	23.9	-1.1	(Russon et al., 2011)
1087 (31S 15E)	18.0	17.7	-0.3	(McClymont et al., 2005)
1123 (41S, 171E)	16.0	16.8	0.8	(Crundwell et al., 2008)
1090 (42S 8E)	11.5	9.8	-1.7	(Martínez-Garcia et al., 2010)